Journal of Molecular Catalysis A: Chemical 303 (2009) 65–71

Contents lists available at ScienceDirect

Journal of Molecular Catalysis A: Chemical

journal homepage: www.elsevier.com/locate/molcata

Study of phase transformation and catalytic performance on precipitated iron-based catalyst for Fischer–Tropsch synthesis

Mingyue Ding[a,b], Yong Yang[a,*], Baoshan Wu[a], Jian Xu[a], Chenghua Zhang[a], Hongwei Xiang[a], Yongwang Li[a]

[a] State Key Laboratory of Coal Conversion, Institute of Coal Chemistry, Chinese Academy of Sciences, Taiyuan 030001, People's Republic of China
[b] Graduate School of the Chinese Academy of Sciences, Beijing 100039, People's Republic of China

ARTICLE INFO

Article history:
Received 21 September 2008
Received in revised form 15 December 2008
Accepted 28 December 2008
Available online 8 January 2009

Keywords:
Fischer–Tropsch synthesis
Iron-based catalyst
Phase transformation
Mössbauer effect spectroscopy

ABSTRACT

Detailed phase transformation in syngas ($H_2/CO = 1.2$) on a precipitated iron-based catalyst was studied by N_2 physisorption, X-ray diffraction (XRD), Mössbauer effect spectroscopy (MES), X-ray photoelectron spectroscopy (XPS) and Raman spectroscopy (LRS). Fischer–Tropsch synthesis (FTS) performance of the catalyst was investigated in a slurry-phase continuously stirred tank reactor (STSR). The hematite in the fresh catalyst was reduced initially to magnetite, and then the magnetite in the bulk reached steady state slowly with increasing reduction time. Simultaneously, the Fe_3O_4 on the surface layers converted gradually to iron carbides, accompanied with the continual increase in the amounts of surface carbonaceous species. In the FTS reaction, the catalytic activity presented an increased trend with gradual carburization of the catalyst by keeping the stability in the bulk Fe_3O_4, suggesting that the conversion of magnetite to iron carbides in the near-surface regions provides probably the active sites for FTS. In addition, the chain growth reaction was restrained and the hydrogenation reaction was enhanced with increasing reduction duration.

1. Introduction

Fischer–Tropsch synthesis (FTS), as an important technology in production of clean transportation fuels and other chemicals from syngas derived from coal, natural gas or biomass [1], has been industrialized in SASOL over 50 years [2]. Due to the limited supplement and rapidly rising price of crude oil, an increasing attention has been renewedly paid on FTS in academic or industrial topic in recent years [3]. Although the Group VIII metals (including Ni, Ru, Co, and Fe) are the most common FTS catalysts, only Fe and Co catalysts have been industrially applied. Compared to Co-based catalyst, iron catalyst is more favorable for converting the syngas with low H_2/CO ratio syngas derived from coal or biomass due to its high water-gas shift (WGS) activity, flexible product distribution and favorable engineering characteristics [4].

Complex phase transformation during pretreatment and reaction from the bulk to surface layers changes directly the Fischer–Tropsch synthesis performances (activity, selectivity and stability). It is well known that the iron oxide (α-Fe_2O_3) is firstly transformed to magnetite (Fe_3O_4) irrespective of the activation gas used, which is then converted to different iron phases depending on the pretreatment parameters. When H_2 is used for activation, the metallic Fe phase is mainly formed, which is readily converted into a mixture of iron carbides (Fe_xC) and Fe_3O_4 under the reaction conditions [5]. Similarly, activation using CO continually transforms the magnetite to different types of iron carbides [6]. In contrast, pretreatment in syngas results in a more complex change in phase compositions, which is difficult to follow as it occurs. Rao et al. [7] investigated activation of a promoted iron-based catalyst and found that pretreatment in syngas for 12.5 h led to the formation of 48% magnetite and 35% carbide phases. The study of Li et al. [8] showed that α-Fe_2O_3 in an un-promoted iron catalyst was firstly reduced to Fe_3O_4 in syngas, and the formed Fe_3O_4 was then gradually carburized with time on stream (TOS). However, the rate of reduction and carburization decreased after activation for 4 h. In addition, variation in pretreatment conditions (temperature, pressure and duration) as well as the reactor system would also cause further change in chemical structure of iron catalysts [9,10]. Due to the extensive phase transformation in syngas over different catalyst systems, understanding of the intrinsic relationship between the FTS performances and microcosmic structures of iron catalyst becomes very difficult [11].

Especially, numerous studies have been performed to investigate the active phases for Fischer–Tropsch synthesis in the working iron catalysts [5,9,11–13]. Some studies indicated that the formation of Fe_3O_4 promoted the FTS activity [12,13], while other

* Corresponding author. Tel.: +86 351 7560835; fax: +86 351 7560668.
E-mail address: yyong@sxicc.ac.cn (Y. Yang).

1381-1169/$ – see front matter © 2009 Elsevier B.V. All rights reserved.
doi:10.1016/j.molcata.2008.12.016

reports claimed that iron carbides were the active phases for FTS [5,11]. Unfortunately, the nature of active sites is still a controversial issue [9]. Additionally, lots of studies reported the appearance of carbonaceous species on the catalyst accompanied with phase transformation during activation and FTS [3,14–18]. Niemantsverdriet et al. [15] claimed that the formation of inactive carbon (graphitic-like) blocked the active sites on the iron carbides, causing the deactivation of a precipitated iron catalyst. However, Ning et al. [3] found that the carbon deposition on mechanically mixed Fe catalysts was not responsible for the changes in catalytic activity. Hence, it needs to further investigate phase evolution from the bulk to surface layers as well as the formation of surface carbonaceous species for illustrating the connection between phase compositions and the FTS performances [10,16].

The objective of the present study was to investigate phase transformation in the bulk and surface layers of a precipitated iron-based catalyst in syngas (H_2/CO = 1.2), and its influence on the FTS performances. Due to the complexity of iron phase compositions, several techniques, including N_2 physisorption, X-ray diffraction (XRD), Mössbauer effect spectroscopy (MES), X-ray photoelectron spectroscopy (XPS) and Raman spectroscopy (LRS), were used together to characterize the textural properties and nature of bulk and surface phases, as well as the carbonaceous species formed on the surface layers.

2. Experimental

2.1. Catalyst preparation

A typical precipitated iron-based catalyst used in the present study was prepared by a combination of co-precipitation and spray drying method. The detailed preparation method has been described elsewhere [19] and protected by Chinese Patent ZL02121248.1 [20]. The freshly prepared catalyst was calcined at 773 K for 5 h.

2.2. Catalyst characterizations

BET surface area, pore volume and average pore diameter of the catalysts were measured by N_2 physisorption at 77 K using a Micromeritics ASAP 2010 instrument. The samples were degassed under vacuum at 393 K for 6 h prior to measurement.

Powder X-ray diffraction (XRD) patterns of the catalyst samples were measured on a D/max-RA X-ray diffractometer (Rigaku, Japan) with Cu Kα radiation (λ = 0.154 nm) operated at 40 kV and 100 mA.

The Mössbauer spectra of catalysts were recorded at room temperature with a MR 351 constant-acceleration Mössbauer spectrometer (FAST, German), using a 25 mCi ^{57}Co (Pd) source. The spectrometer was operated in a symmetric constant acceleration mode. The spectra were collected over 512 channels in the mirror image format.

In situ XPS experiments were performed in an atmospheric quartz tube flow reactor, using He as the carrier gas. The feed gas with H_2/CO ratio of 1.2 passed through a series of columns for removing tiny amounts of oxygen, sulfur, carbonyls and water. The gas flow rate was 60 ml/min and the catalyst was pretreated at 538 K and 0.50 MPa for different durations. After pretreatment the sample was cooled in the carrier gas to room temperature, and then transferred into the ultra-high vacuum chamber (UHV) without exposure to air. XPS spectra were taken by a VG MiltiLab 2000 system with Al Kα (1486.6 eV) as the X-ray source. The C 1s as a reference signal was adjusted to 284.6 eV.

Raman spectra of the catalyst samples were collected using a single monochromator Renishaw system 1000 equipped with a thermoelectrically cooled CCD detector and holographic super-notch filter. The sample was excited with the 514.5 nm Ar line, and the spectrum acquisition time was 50 s. The spectra were recorded in the range between 100 and 1800 cm^{-1}.

Table 1
Textural properties of the catalysts reduced for different durations.

Run no.	BET surface area (m^2/g)	Pore volume (cm^3/g)	Average pore size (nm)
T12	91	0.23	10.10
T36	72	0.22	11.90
T72	73	0.22	12.11

Reduction conditions: H_2/CO = 1.2, 538 K, 0.50 MPa and 1000 h^{-1}.

2.3. Reactor system and pretreatment procedures

The FTS tests were carried out in a 1 dm^3 slurry-phase continuously stirred tank reactor (STSR) loaded with 20.0 g of the catalyst sample and 380 g of liquid paraffin. The H_2 and CO were passed separately through a series of columns, an activated charcoal trap, an oxygen-removal trap, a sulfur-removal trap and a silica-gel/5 A molecular sieve trap, to remove tiny amounts of carbonyls, oxygen, sulfur and water before entering the reactor. The flow rates of H_2 and CO were controlled by two mass flow meters (Brooks 5850E). The outlet of the reactor was connected with a hot trap (393 K) and a cold trap (273 K) at the system pressure. A wet gas flow meter was used to monitor the flow rate of tail gas. All activations were conducted in situ in syngas (H_2/CO = 1.2), at 538 K, 1000 h^{-1}, 0.50 MPa and different durations (12, 36 and 72 h). These tests were labeled as T12, T36 and T72, respectively. After reduction, steady-state reaction conditions were set as 533 K, 1.50 MPa, 2000 h^{-1} and H_2/CO = 1.2. Detailed description of the reactor and product analyst systems have been provided elsewhere [21].

3. Results and discussion

3.1. Textural properties of the catalysts

The textural properties of the catalysts during various reduction durations are listed in Table 1. The BET surface area, pore volume and average pore size of the fresh catalyst are 166 m^2/g, 0.36 cm^3/g and 8.55 nm, respectively. The BET surface area of the catalyst firstly decreased with TOS during pretreatment and then kept nearly unchanged (72–73 m^2/g) after reduction for 36 h. The phenomenon implies that the structure of the catalyst undergoes marked changes during the initial stage of reduction, possibly resulting from partial collapse of the porous of iron oxide network [2], and then the bulk structure of the catalyst might reach a stable state after 36 h of reduction. The combination of XRD and MES measurements (in the following section) showed that the amount of magnetite formed in the bulk increased gradually and then reached nearly steady-state values after 36 h of reduction, suggesting that the steady-state bulk Fe_3O_4 maybe the main contribution to the structure stability for the catalyst.

3.2. Phase transformation of the catalysts

3.2.1. Phase transformation during reduction

The XRD and MES patterns of the fresh catalyst and reduced samples in syngas (H_2/CO = 1.2) at 538 K, 0.50 MPa and 1000 h^{-1} for different durations are showed in Figs. 1 and 2, respectively. The corresponding iron-phase compositions of the catalysts are listed in Table 2. As described in the previous study [22], the fresh catalyst is mainly composed of α-Fe_2O_3. After reduction, the XRD patterns of the samples (Fig. 1) show several diffraction peaks at 2θ values of 30.0°, 35.4°, 57.0° and 62.6°, all of which correspond to Fe_3O_4. In

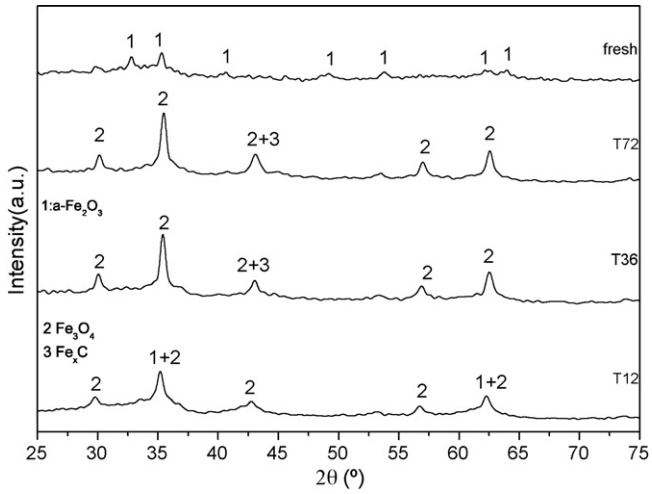

Fig. 1. XRD patterns of the catalysts reduced for different durations. (1) α-Fe_2O_3, (2) Fe_3O_4 and (3) Fe_xC. Reduction conditions: $H_2/CO = 1.2$, 538 K, 0.50 MPa and 1000 h^{-1}.

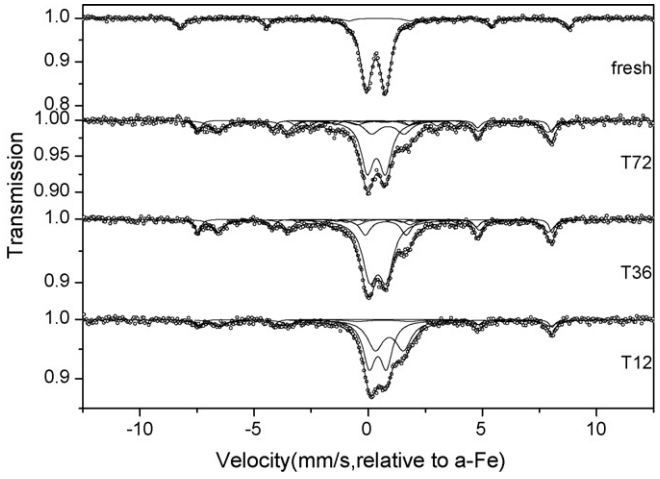

Fig. 2. Mössbauer spectra of the catalysts reduced for different durations. Reduction conditions: $H_2/CO = 1.2$, 538 K, 0.50 MPa and 1000 h^{-1}.

Table 3
Analysis of XRD and MES patterns of the catalysts reduced for different durations.

Run no.	Ratio of XRD peak at 35.4° to that at 43°	Carbide/(carbide + magnetite) (%)	
		XRD	MES
T12	3.26	2.2	–
T36	2.61	21.7	19.4
T72	2.32	30.4	27.9

addition, a broad diffraction peak centered at 43° was observed for all samples, corresponding to the overlap of Fe_3O_4 and iron carbides according to the data of JCPDS [23]. Apparently, the peak intensity of magnetite increased gradually with TOS and then reached slowly a steady state after 36 h of reduction, indicating that with time on stream the hematite converts gradually to the magnetite, and then the formed Fe_3O_4 in the bulk keeps unchanged slowly. In addition, the intensity of diffraction peak at 43° increased slightly with increasing reduction time. Datye and coworkers [9] used the peak area to reflect the intensity of each phase as a qualitative measure of the amount of that phase, because the quantitative identification of various phases is impossible according to the XRD analysis. Therefore, we used the ratio of the peak at 35.4° with the 43° peak as an estimate of the percentage of carbide in the sample. The calculational results of XRD profiles are shown in Table 3. It is apparent that the amount of iron carbides presented an increased trend as a function of duration time.

The results of MES measurements (Fig. 2 and Table 2) showed that 21.6% and 36.0% Fe^{3+} were transformed to Fe_3O_4 and superparamagnetic (spm) Fe^{2+} after 12 h of reduction, respectively. Thereafter, the amount of bulk magnetite increased gradually and then reached lowly a steady-state value (about 32%) after reduction for 36 h, simultaneously, accompanied with the slow formation of iron carbides. The result is in well agreement with that of XRD. The formation of metallic iron was not observed for longer reduction time, indicating that metallic iron might not an intermediate for converting Fe_3O_4 to Fe_xC [8]. The MES results of carbide and magnetite in phase compositions are also listed in Table 3. It can be found that the ratio of carbide to Fe_3O_4 in the bulk obtained from the analysis of XRD is consistent with the value of MES calculation in the error range of ±5%, indicating that the contents of iron carbides and Fe_3O_4 in paramagnetic state detected by MES reflect actually the diffraction intensity of iron phases. Furthermore, the gradual increase in the amount of Fe_xC by keeping the stable state in bulk Fe_3O_4 implies that the formation of carbide phase maybe originates from the conversion of Fe_3O_4

Table 2
Iron-phase composition of the catalysts at different states.

Run no.	T12		T36		T72	
	Phase	Area (%)	Phase	Area (%)	Phase	Area (%)
After reduction	Fe_3O_4	21.6	Fe_3O_4	31.6	Fe_3O_4	32.9
	(spm) Fe^{3+}	42.4	χ-Fe_5C_2	7.6	χ-Fe_5C_2	6.0
	(spm) Fe^{2+}	36.0	(spm) Fe^{3+}	49.6	ε'-$Fe_{2.2}C$	6.7
			(spm) Fe^{2+}	11.2	(spm) Fe^{3+}	40.7
					(spm) Fe^{2+}	13.7
Reaction for 6 h	Fe_3O_4	28.2	Fe_3O_4	32.9	Fe_3O_4	31.2
	χ-Fe_5C_2	1.1	χ-Fe_5C_2	4.7	χ-Fe_5C_2	5.6
	(spm) Fe^{3+}	52.3	ε'-$Fe_{2.2}C$	3.2	ε'-$Fe_{2.2}C$	7.8
	(spm) Fe^{2+}	18.4	(spm) Fe^{3+}	55.9	(spm) Fe^{3+}	36.9
			(spm) Fe^{2+}	3.3	(spm) Fe^{2+}	18.5
Reaction for 500 h	Fe_3O_4	36.3	Fe_3O_4	31.7	Fe_3O_4	32.7
	χ-Fe_5C_2	4.6	χ-Fe_5C_2	10.3	χ-Fe_5C_2	14.1
	ε'-$Fe_{2.2}C$	1.5	(spm) Fe^{3+}	40.1	(spm) Fe^{3+}	33.7
	(spm) Fe^{3+}	47.7	(spm) Fe^{2+}	17.9	(spm) Fe^{2+}	19.4
	(spm) Fe^{2+}	9.8				

Reduction conditions: $H_2/CO = 1.2$, 538 K, 0.50 MPa and 1000 h^{-1}.
Reaction conditions: $H_2/CO = 1.2$, 533 K, 1.50 MPa and 2000 h^{-1}.

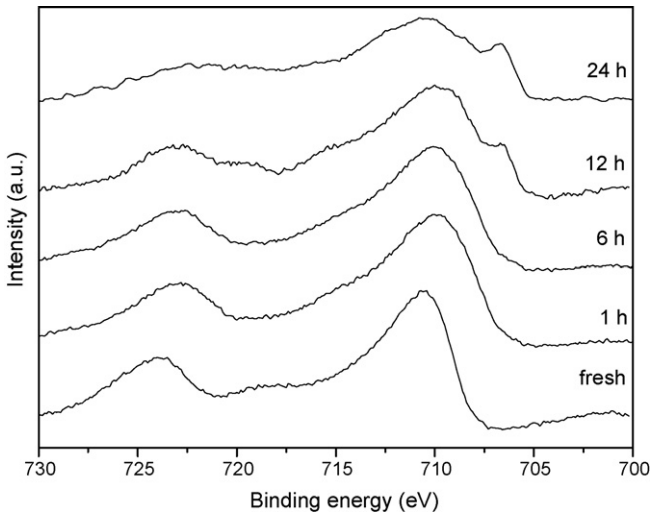

Fig. 3. XPS spectra of the catalysts reduced for different durations in Fe 2p region. Reduction conditions: $H_2/CO = 1.2$, 538 K, 0.50 MPa and 60 ml/min.

on the surface layers. To further confirm the process of converting Fe_3O_4 to Fe_xC, XPS was used to investigate phase transformation in the near-surface regions as a function of reduction time.

Figs. 3 and 4 show the XPS spectra in the Fe 2p and C 1s regions of the catalysts after in situ pretreatment in syngas ($H_2/CO = 1.2$) at 538 K, 0.50 MPa, 60 ml/min for different durations, respectively. As shown in Fig. 3, the Fe $2P_{3/2}$ peak in the fresh catalyst corresponding to Fe_2O_3 [24]. After reduction for 1 h, the Fe $2P_{3/2}$ peak became broader and shifted towards lower binding energies, which could be attributed to the presences of both Fe^{2+} and Fe^{3+} in Fe_3O_4 [25]. A weak shoulder peak appeared at 715.4 eV, which indicates the presence of reduced Fe^{2+} [24]. For the catalysts being reduced over 6 h, a narrow peak appeared at 706.7 eV besides the presence of the magnetite peak, which corresponding to the appearance of carbide phase [17,24]. XPS characterization showed that the hematite in the near-surface regions was rapidly converted to magnetite after reduction for 1 h. Thereafter, the amount of magnetite decreased gradually with increasing time, while that of iron carbides presented an increased trend, suggesting that the hematite on the surface layers was firstly reduced to Fe_3O_4, and then gradually carburized to iron carbides. In addition, the formation of carbonaceous species was also observed on the catalyst. As shown in Fig. 4,

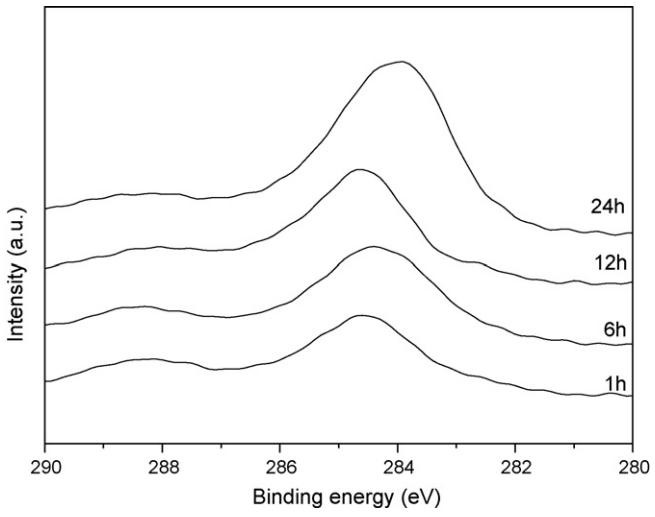

Fig. 4. XPS spectra of the catalysts reduced for different durations in C 1s region. Reduction conditions: $H_2/CO = 1.2$, 538 K, 0.50 MPa and 60 ml/min.

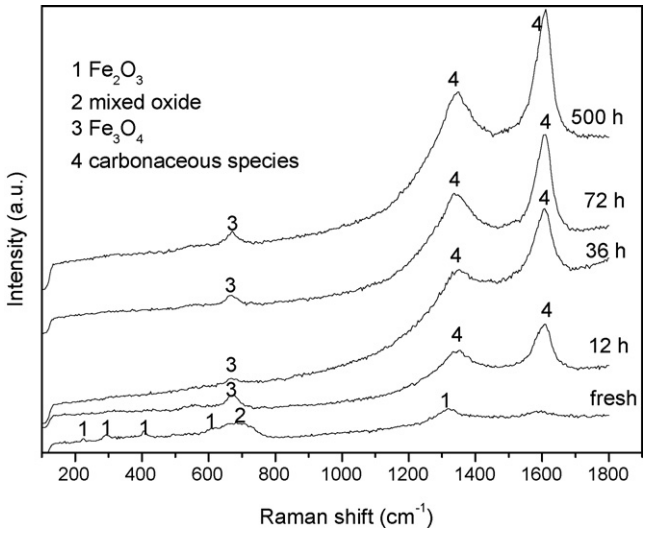

Fig. 5. Raman spectra of the catalysts at different states. Reduction conditions: $H_2/CO = 1.2$, 538 K, 0.50 MPa and 1000 h^{-1}. Reaction conditions: $H_2/CO = 1.2$, 533 K, 1.50 MPa and 2000 h^{-1}.

a main peak at about 284.6 eV is ascribed to the formation of surface carbon. It is apparent that the peak intensity of surface carbon presented an increased trend with TOS, indicating that longer reduction duration facilitates the formation of surface carbonaceous species.

To further investigate the influence of reduction time on surface carbonaceous species in STSR, the samples during reduction and FTS were characterized by LRS. As shown in Fig. 5, the spectra of the fresh catalyst mainly comprise of the peaks of α-Fe_2O_3 phase [26]. In addition, a broad peak at 688 cm^{-1} is ascribed to the formation of mixed oxide [27]. For the catalysts reduced for different durations and the sample after reaction in STSR, there are three peaks in the Raman spectra profiles. A weak peak appeared at 669 cm^{-1} is ascribed to the magnetite phase [26], and two broad peaks at 1346 and 1608 cm^{-1} can be attributed to the appearance of the disordered (D band) and ordered (G band) carbonaceous species [28]. Apparently, the carbonaceous species were formed gradually on the catalyst with time on stream during reduction and FTS, which is consistent with the results of XPS. Datye and coworkers [9] observed the formation of amorphous carbon layers on the iron carbide particles during FTS over precipitated iron catalyst by TEM and XPS. They later reported that changes in reduction temperature determined the nature of carbonaceous species over Fe/SiO_2 catalyst in CO [29]. Pretreatment in CO at 653 K resulted in the formation of amorphous carbon layers, whereas large amounts of graphitic carbon layers were observed at 773 K in carbon monoxide. Therefore, they suggested that the amorphous carbonaceous compounds were mainly formed on the catalyst surface in CO or syngas at lower temperatures. Compared to the results of Datye and coworkers, our tests were undertaken in syngas at 538 K. At such a low temperature, the carbonaceous species formed on the surface layers of the catalyst in STSR could mainly be attributed to the amorphous carbonaceous compounds.

3.2.2. Phase transformation during reaction

The XRD and MES patterns of the used catalysts in syngas ($H_2/CO = 1.2$) at 533 K, 1.50 MPa and 2000 h^{-1} for 6 h are shown in Figs. 6 and 7, respectively. The corresponding iron-phase compositions of the catalysts are listed in Table 2. As shown in Fig. 6, there are mainly the diffraction peaks of Fe_3O_4 and iron carbides in the XRD patterns. No obvious difference was observed for the magnetite intensity of all catalyst samples, whereas the intensity of iron carbides increased slightly following the order in runs T12, T36 and

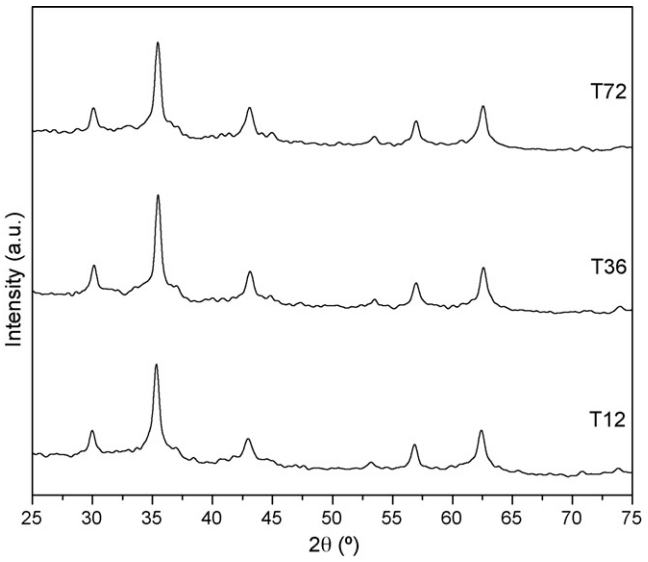

Fig. 6. XRD patterns of the catalysts after reaction for 6 h. Reaction conditions: $H_2/CO = 1.2$, 533 K, 1.50 MPa and 2000 h^{-1}.

T72. From the results of MES (Fig. 7 and Table 2), it can be found that during the initial stages of reaction the amount of Fe_3O_4 in all samples was equivalent basically, while that of iron carbides in the catalyst reduced for longer time was higher, which is in well agreement with the results of XRD. Compared with the reduced catalysts, the amounts of Fe_3O_4 and Fe_xC in run T12 increased slowly after the starting of reaction, while that of magnetite remained constant nearly for the samples in runs T36 and T72, accompanied by the slight increase in Fe_xC content. This indicates that the catalyst being reduced for 12 h is not completely reduced and carburized, while pretreatments for 36 h and above result in the complete reduction from hematite to magnetite. Therefore, the bulk Fe_3O_4 being reduced over 36 h continues to remain steady state during the early stages of reaction. The slight increase in Fe_xC content as the bulk magnetite remains unchanged might stem from the conversion of magnetite on the surface layers.

During the steady-state reaction (Fig. 8) the bulk structure of the samples in runs T36 and T72 continued to remained constant

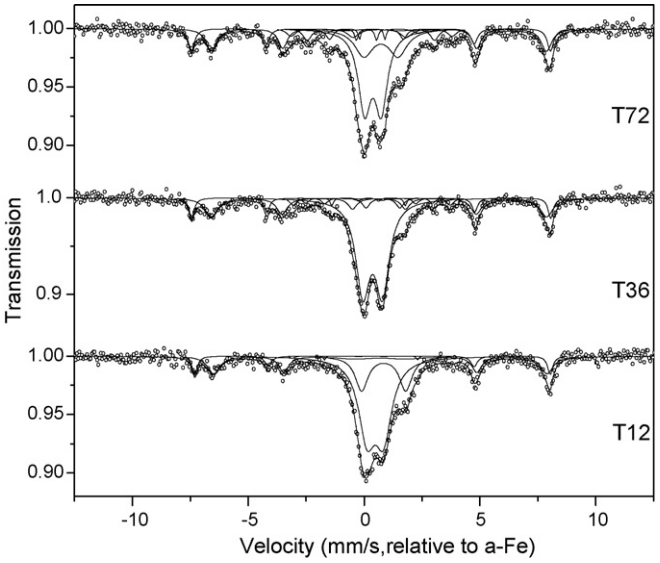

Fig. 7. Mössbauer spectra of the catalysts after reaction for 6 h. Reaction conditions: $H_2/CO = 1.2$, 533 K, 1.50 MPa and 2000 h^{-1}.

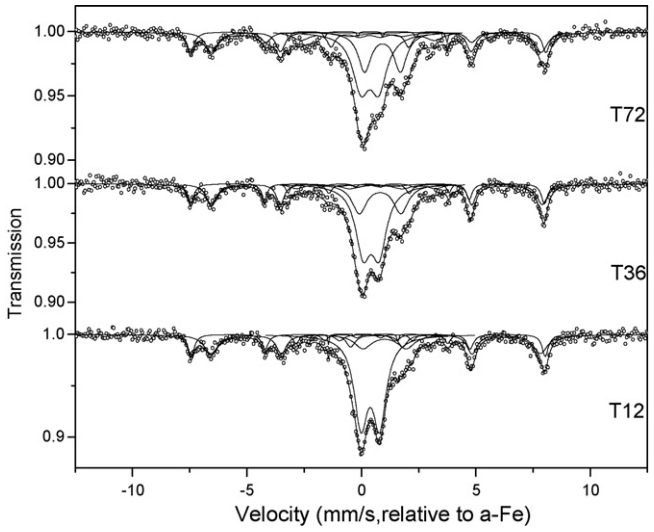

Fig. 8. Mössbauer spectra of the catalysts after reaction for 500 h. Reaction conditions: $H_2/CO = 1.2$, 533 K, 1.50 MPa and 2000 h^{-1}.

nearly, accompanied with the slightly increase in Fe_xC content, indicating that with TOS during FTS the magnetite on the surface layers converts continually to iron carbides. Moreover, it is also found that there exists the transformation of ε'-$Fe_{2.2}C$ to χ-Fe_5C_2 phase during FTS (Table 2). Niemantsverdriet et al. [15] reported that the ε'-$Fe_{2.2}C$ phase was only detected in silica-supported iron catalysts with syngas at low temperature (513 K). It is possible that the ε'-$Fe_{2.2}C$ phase is not stable and converts to more stable χ-Fe_5C_2 phase at relative high reaction temperature (533 K) by the removal of carbon.

3.3. FTS performances of the catalysts

The FTS performances of the catalysts were measured in STSR under reaction conditions of 533 K, 1.50 MPa, 2000 h^{-1} and $H_2/CO = 1.2$. The activities, stabilities and product selectivities were tested over a period of 500 h steady-state runs.

3.3.1. Activity and stability

Fig. 9 shows the conversions and stabilities for the FTS reaction of the catalysts being pretreated with different durations. It

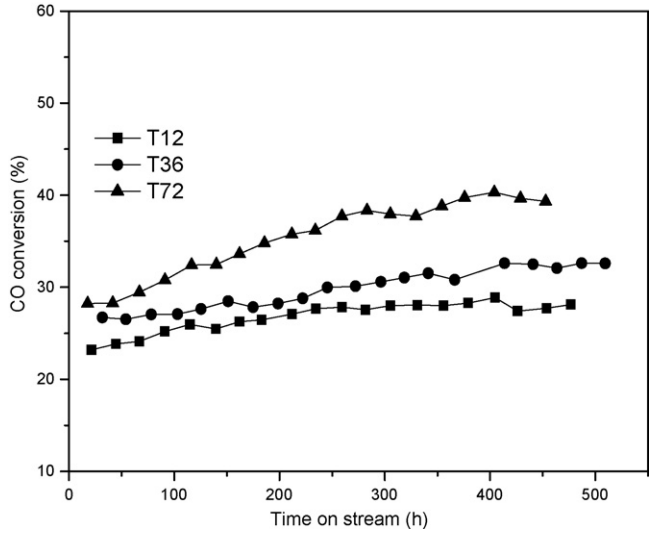

Fig. 9. CO conversion of the catalysts reduced for different durations. Reaction conditions: $H_2/CO = 1.2$, 533 K, 1.50 MPa and 2000 h^{-1}.

Table 4
Performances of the catalysts reduced for different durations.

	Run no. TOS (h)								
	T12			T36			T72		
	234	355	477	199	296	509	211	329	453
CO conversion (mol %)	27.67	28.01	28.11	28.24	30.60	32.59	35.75	37.73	39.33
$CO + H_2$ conversion (mol %)	28.63	29.22	29.36	28.08	30.46	32.31	33.59	35.41	36.06
CO_2 selectivity (mol%) (C basis)	25.94	27.62	24.97	35.59	34.81	35.01	35.92	36.87	38.22
WGS ($P_{CO_2}P_{H_2}/P_{CO}P_{H_2O}$)	0.81	0.90	0.82	1.11	1.18	1.24	1.44	1.54	1.69
H_2/CO in tail gas	1.17	1.16	1.16	1.20	1.20	1.23	1.28	1.29	1.32
H_2/CO usage	1.28	1.30	1.30	1.18	1.18	1.15	1.07	1.07	1.02
Hydrocarbon selectivity (wt%)									
C_1	8.33	8.54	8.90	9.61	9.44	10.03	10.04	10.06	10.59
C_{2-4}	31.56	31.23	31.90	32.33	32.93	33.80	34.03	34.57	35.33
C_{5-11}	40.95	40.98	39.96	39.75	39.17	38.48	40.56	40.43	40.42
C_{12}^+	19.16	19.26	19.24	18.32	18.46	17.69	15.37	14.94	13.66
Olefin content (wt%)									
C_{2-4}	81.16	79.99	79.63	79.47	79.18	78.87	78.69	78.21	77.23
C_{5-11}	79.11	78.35	78.86	78.90	77.35	77.18	77.89	77.74	77.76

Reaction conditions: $H_2/CO = 1.2$, 533 K, 1.50 MPa and 2000 h^{-1}.

is apparent that changes in phase composition strongly influenced the catalytic activity. The catalyst in run T72 showed the highest initial catalytic activity, followed by the catalyst in run T36, while the catalyst in run T12 showed the lowest FTS activity. During the reaction for about 500 h, CO conversions increased slightly with time on stream from 23 and 26% to 28 and 32% for the catalysts in runs T12 and T36, respectively. In contrast, CO conversion of the catalyst in run T72 increased remarkably from 28 to 39% as a function of reaction time.

According to the results on phase compositions in the bulk and surface layers, it is known that the hematite in the fresh catalyst reduced firstly to the magnetite as a function of time, and then the formed Fe_3O_4 in the bulk reached gradually the steady state. In contrast, the magnetite on the surface layers converted monotonously to iron carbides with increasing reduction time. Similarly, the catalytic activity presented an increased trend with the increase in reduction time. Furthermore, with gradual carburization of the catalyst in the near-surface regions during FTS via keeping the stable state in bulk Fe_3O_4, the catalyst activity increased in parallel with time on stream. Li et al. [30] reported that only a fraction of iron carbides on the surface layers promotes the catalytic activity in the FTS reaction. Therefore, it is possible that the gradual conversion of magnetite to iron carbides on the surface layers provides the active sites for FTS, promoting the catalytic activity, regardless of the chemical nature of the residual bulk Fe_3O_4 or carbides.

On the other hand, the carbonaceous species were formed on the catalyst and the amounts of these species increased with TOS during reduction and FTS, accompanied synchronously with the slight increase in catalyst activity. This indicates that the formation of carbonaceous species on the catalyst does not suppress the catalytic activity. Some studies suggested that the carbon deposition was one of the reasons to decrease the FTS activity over iron-based catalysts [15,17,18], while others indicated that the formation of carbonaceous species on the catalyst did not restrain the catalyst activity [3,14,16]. Dwyer and Hardenbergh suggested that the deactivation of the catalyst was associated with the formation of graphite-type carbonaceous compounds [17]. As the Raman spectra results shown, carbonaceous species formed on the catalyst during reduction and reaction were mainly attributed to the amorphous carbonaceous compounds. Since there is no obvious formation of graphite type carbonaceous compounds, these amorphous carbonaceous species formed may be mere spectators, which does not impair the catalyst activity in the measuring period of about 500 h.

3.3.2. Product selectivity

The hydrocarbon selectivities of all catalysts are shown in Table 4. It can be seen that the selectivities to gaseous hydrocarbons (methane and C_2–C_4) were enhanced, whereas those to heavy hydrocarbons (C_{12}^+) and olefins ($C_2^=$–$C_4^=$ and $C_5^=$–$C_{11}^=$) were suppressed with the increase in reduction time, indicating that the chain growth reaction is inhibited and the hydrogenation reaction of olefins is enhanced with increasing reduction time. It is well known that potassium as an effective promoter could increase the strength of CO chemisorption, suppress H_2 adsorption, facilitate chain growth reaction and enhance selectivities to heavy hydrocarbons and olefins [31,32]. With the gradual formation of carbon depositions on the surface the potassium might migrate to the surface of these carbonaceous species, weakening the contact of Fe/K and reducing the effective potassium content in the near-surface regions. Consequently, the decrease in effective potassium content might lead to the decrease in CO adsorption concentration and the increase in H_2 adsorption on the catalyst, facilitating the shift of the product distribution towards lower molecular weight hydrocarbons as well as promoting the hydrogenation reaction of olefins.

4. Conclusions

In the present study, combined methods (BET, XRD, MES, XPS and LRS) were applied to characterize the textural properties, bulk/surface phase compositions of a precipitated iron-based catalyst during different stages of reduction and reaction. The surface area of the catalyst decreased firstly and then reached gradually a stable state with the increase in reduction time. Simultaneously, the hematite in the fresh catalyst was initially reduced to magnetite and the amount of magnetite in the bulk also slowly remained unchanged. With time on stream during reduction iron carbides were progressively formed via the conversion of the magnetite on the surface layers, accompanied with the gradual increase in carbonaceous species concentration on the catalyst.

During the FTS reaction the initial catalytic activity was the lowest as the catalyst was mainly reduced to magnetite, and it increased gradually with the slight carburization of the catalyst by keeping the stable magnetite in the bulk, suggesting that the formation of iron carbides on the surface layers might provide the active sites for FTS. In addition, increasing reduction time in syngas facilitated the product distributions shifting towards lower molecular weight hydrocarbons and the hydrogenation reaction of olefins.

Acknowledgements

The authors gratefully acknowledge the financial support from Key Program of National Outstanding Young Scientists Foundation of China (20625620), National Key Basic Research Program of China (2007CB216401). This work is also supported by Synfuelschina Co., Ltd.

References

[1] D.S. Kalakkad, M.D. Shroff, S. Köhler, N. Jackson, A.K. Datye, Appl. Catal. A: Gen. 133 (1995) 335.
[2] R.B. Anderson, The Fischer–Tropsch Synthesis, Academic Press, Orlando, FL, 1984.
[3] W.S. Ning, N. Koizumi, M. Yamada, Catal. Commun. 8 (2007) 275.
[4] M.E. Dry, J. Chem. Technol. Biotechnol. 77 (2001) 43.
[5] G.B. Raupp, W.N. Delgass, J. Catal. 58 (1979) 348.
[6] C.S. Huang, B. Ganguly, G.P. Huffman, F.E. Huggins, B.H. Davis, Fuel Sci. Technol. Int. 11 (1993) 1289.
[7] K.R.P.M. Rao, F.E. Huggins, G.P. Huffman, R.J. O'Brien, R.J. Gormley, B.H. Davis, Fuel Chem. 40 (1995) 153.
[8] S. Li, G.D. Meitzner, E. Iglesia, J. Phys. Chem. B 105 (2001) 5743.
[9] M.D. Shroff, D.S. Kalakkad, K.E. Coulter, S.D. Köhler, M.S. Harrington, N.B. Jackson, A.G. Sault, A.K. Datye, J. Catal. 156 (1995) 185.
[10] R.J. O'Brien, L. Xu, D.R. Milburn, Y.X. Li, K.J. Klabunde, B.H. Davis, Top. Catal. 2 (1995) 1.
[11] M.V. Cagnoli, N.G. Gallegos, A.M. Alvarez, J.F. Bengoa, A.A. Yeramián, M. Schmal, S.G. Marchetti, Appl. Catal. A: Gen. 230 (2002) 169.
[12] J.B. Butt, Catal. Lett. 7 (1991) 61.
[13] C.S. Kuivila, P.C. Stair, J.B. Butt, J. Catal. 118 (1989) 299.
[14] W.S. Ning, N. Koizumi, H. Chang, T. Mochizuki, T. Itoh, M. Yamada, Appl. Catal. A: Gen. 312 (2006) 35.
[15] J.W. Niemantsverdriet, A.M. van der Kraan, W.L. van Dijk, H.S. van der Baan, J. Phys. Chem. 84 (1980) 3363.
[16] T. Herranz, S. Rojas, F.J. Perez-Alonso, M. Ojeda, P. Terreros, J.L.G. Fierro, J. Catal. 243 (2006) 199.
[17] D.J. Dwyer, J.H. Hardenbergh, J. Catal. 87 (1984) 66.
[18] A. Loaiza-Gil, B. Fontal, F. Rueda, J. Mendialdua, R. Casanova, Appl. Catal. A: Gen. 177 (1999) 193.
[19] Y. Yang, H.W. Xiang, L. Tian, H. Wang, C.H. Zhang, Z.C. Tao, Y.Y. Xu, B. Zhong, Y.W. Li, Appl. Catal. A 284 (2005) 105.
[20] H. Xiang, Y. Yang, Y. Li, L. Bai, B. Zhong, C.N. Patent ZL02121248.1.
[21] C.H. Zhang, Y. Yang, B.T. Teng, T.Z. Li, H.Y. Zheng, H.W. Xiang, Y.W. Li, J. Catal. 237 (2006) 405.
[22] M. Ding, Y. Yang, J. Xu, Z. Tao, H. Wang, H. Wang, H. Xiang, Y. Li, Appl. Catal. A: Gen. 345 (2008) 176.
[23] Joint Committee for Powder Diffraction Standards, "JCPDS", International Center for Diffraction Data, 1979.
[24] C.S. Kuivila, J.B. Butt, P.C. Stair, Appl. Surf. Sci. 32 (1988) 99.
[25] D.B. Bukur, K. Okabe, M.P. Rosynek, C. Li, D. Wang, K.R.P.M. Rao, G.P. Huffman, J. Catal. 155 (1995) 353.
[26] D.L.A. Faria, S.V. Silva, M.T. Oliveira, J. Raman Spectrosc. 28 (1997) 873.
[27] T. Herranz, S. Rojas, M. Ojeda, F.J. Pérez-Alonso, P. Terreros, K. Pirota, J.L.G. Fierro, Chem. Mater. 18 (2006) 2364.
[28] S.M.K. Airaksinen, M.A. Banares, A.O.I. Krause, J. Catal. 230 (2005) 507.
[29] Y. Jin, A.K. Datye, J. Catal. 196 (2000) 8.
[30] S. Li, W. Ding, G.D. Meitzner, E. Iglesia, J. Phys. Chem. B 106 (2002) 85.
[31] H. Kölbel, H. Giehring, Brennstoff-Chem. 44 (1963) 343.
[32] D.B. Bukur, D.S. Mukesh, A. Patal, Ind. Eng. Chem. Res. 29 (1990) 194.